Journal of Biomechanics 89 (2019) 85–94

Contents lists available at ScienceDirect

Journal of Biomechanics

journal homepage: www.elsevier.com/locate/jbiomech
www.JBiomech.com

Adaptive changes in micromechanical environments of cancellous and cortical bone in response to in vivo loading and disuse

Haisheng Yang [a,*], Xiaoyu Xu [b,c], Whitney Bullock [d], Russell P. Main [b,c]

[a] Department of Biomedical Engineering, School of Life Science and Bioengineering, Beijing University of Technology, Intelligent Physiological Measurement and Clinical Translation Beijing International Base for Scientific and Technological Cooperation, Beijing, China
[b] Musculoskeletal Biology and Mechanics Lab, Department of Basic Medical Sciences, Purdue University, IN, USA
[c] Weldon School of Biomedical Engineering, Purdue University, IN, USA
[d] School of Medicine, Indiana University, IN, USA

ARTICLE INFO

Article history:
Accepted 12 April 2019

Keywords:
In vivo tibial loading
Hindlimb unloading
Bone adaptation
microCT
Finite element analysis

ABSTRACT

The skeleton accommodates changes in mechanical environments by increasing bone mass under increased loads and decreasing bone mass under disuse. However, little is known about the adaptive changes in micromechanical behavior of cancellous and cortical tissues resulting from loading or disuse. To address this issue, in vivo tibial loading and hindlimb unloading experiments were conducted on 16-week-old female C57BL/6J mice. Changes in bone mass and tissue-level strains in the metaphyseal cancellous and midshaft cortical bone of the tibiae, resulting from loading or unloading, were determined using microCT and finite element (FE) analysis, respectively. We found that loading- and unloading-induced changes in bone mass were more pronounced in the cancellous than cortical bone. Simulated FE-loading showed that a greater proportion of elements experienced relatively lower longitudinal strains following load-induced bone adaptation, while the opposite was true in the disuse model. While the magnitudes of maximum or minimum principal strains in the metaphyseal cancellous and midshaft cortical bone were not affected by loading, strains oriented with the long axis were reduced in the load-adapted tibia suggesting that loading-induced micromechanical benefits were aligned primarily in the loading direction. Regression analyses demonstrated that bone mass was a good predictor of bone tissue strains for the cortical bone but not for the cancellous bone, which has complex microarchitecture and spatially-variant strain environments. In summary, loading-induced micromechanical benefits for cancellous and cortical tissues are received primarily in the direction of force application and cancellous bone mass may not be related to the micromechanics of cancellous bone.

1. Introduction

Mechanical stimuli play a key role in bone (re)modeling for maintenance of the skeleton to resist fracture during habitual loading. It has been demonstrated that bone (re)modeling is sensitive to changes in habitual mechanical loading. For example, enhanced mechanical stimuli (e.g. exercise) can improve bone mass while reduced mechanical stimuli (e.g. space flight or prolonged bed-rest conditions) may lead to bone loss (Gerbaix et al., 2017; Haapasalo et al., 2000).

Experimental animal models have been widely used to study the effects of mechanical loading or unloading on bone tissue and to reveal the underlying mechanobiological mechanisms regulating bone adaptation. In vivo loading models have been essential in establishing the relationships between mechanical signals and osteogenesis (Meakin et al., 2014; Robling et al., 2001; Turner, 1998). Early models enabling extrinsic control of load levels typically employed invasive surgical procedures, such as pinning and external fixation (Lanyon and Rubin, 1984; Rubin and Lanyon, 1984), which could potentially induce infection and inflammation and thus affect the interpretation of results (Bertram and Swartz, 1991). Non-invasive loading models, such as four-point bending and cantilever bending of rodent tibiae and compressive loading of ulnae, were developed (Baumann et al., 2015; Gross et al., 2002; Robling et al., 2002). However, those models were mainly used to investigate cortical bone response to loading. The in vivo

* Corresponding author at: Department of Biomedical Engineering, School of Life Science and Bioengineering, Beijing University of Technology, 100 Pingleyuan, Chaoyang District, Beijing 100124, China.
E-mail addresses: haisheng.yang@bjut.edu.cn (H. Yang), xu966@purdue.edu (X. Xu), bullockw@umail.iu.edu (W. Bullock), rmain@purdue.edu (R.P. Main).

https://doi.org/10.1016/j.jbiomech.2019.04.021
0021-9290/

mouse tibial axial compression loading model was developed to investigate mechanical adaptation simultaneously in cancellous and cortical bone tissues (De Souza et al., 2005; Fritton et al., 2005; Silva et al., 2012). This model can induce a more physiological strain distribution throughout the tibia compared to prior avian and rodent models (Meakin et al., 2014). Conversely, the most common in vivo unloading model used to achieve a mechanical disuse environment for hindlimbs is tail suspension. This model induces significant bone loss in both cancellous and cotical bone in the hind limbs (Morey-Holton and Globus, 2002; Robling et al., 2008).

The majority of studies have investigated the effect of loading or unloading on bone adaptation using micro-computed tomography (microCT), dynamic histomorphometry and/or in vivo microCT/fluorochrome-based 3D morphometry (Javaheri et al., 2018; Carriero et al., 2018; De Souza et al., 2017; Lynch et al., 2010; Sugiyama et al., 2012; Birkhold et al., 2014; Razi et al., 2015a; Birkhold et al., 2017). These outcome measures are important to assess how and where bone forms or resorbs in response to loading or unloading as well as to determine the spatial relations between mechanical stimuli and bone responses (Carriero et al., 2018; Javaheri et al., 2018; Razi et al., 2015a; Robling et al., 2008). However, a beneficial or detrimental functional outcome of loading or unloading is ultimately determined by bone's mechanical performance, including its tissue-level micromechanical behavior and apparent-level bone strength. In addition to microCT and histomorphometry, some studies conducted three- or four-point bending to evaluate the effect of loading on apparent mechanical behavior of a whole bone and showed a load-induced improvement in bone strength (Berman et al., 2015; Robling et al., 2002). Others used strain gauges placed on the medial surface of the tibial midshaft to measure the in vivo stiffness and found a load-induced increase in stiffness in 6-week-old mice but a decrease in 16-week-old mice (Main et al., 2014). Finite element (FE) modeling in combination with strain gauging and/or digital image correlation (DIC) has been adopted as robust methods to determine the pre-adapted cortical and cancellous strains engendered by applied load (Lambers et al., 2015; Patel et al., 2014; Razi et al. 2015a; Razi et al., 2015b; Yang et al., 2014; Carriero et al., 2014; Pereira et al., 2015). DIC has also been used to measure surface strains on post-adapted cortical bones (Sztefek et al., 2010). So far, relatively little is known about the adaptive changes in micromechanical environments within the cancellous and cortical bone following loading or unloading, which may not be proportional to bone mass changes but could be important for understanding the biomechanical outcomes of bone adaptation.

Therefore, the goal of this study was to examine the loading- or unloading-induced alterations in tissue-level mechanical environments of cancellous and cortical bone using in vivo mouse tibial loading and hindlimb unloading models. We hypothesized that loading-induced bone adaptation would lead to a decrease in tissue strain due to an increase in bone mass while decreased bone mass with disuse would result in increased bone strains. Changes in bone mass and tissue-level strain environments resulting from loading (or unloading) were determined using microCT and a previously validated FE modeling approach (Yang et al., 2017a; Yang et al., 2014), respectively.

2. Materials and methods

2.1. Study design and animals

Sixteen-week-old female C57BL/6J mice were used in this study. Two individual experiments were conducted. For the loading experiment, one group of mice underwent in vivo tibial compressive loading for two weeks with the left limb being loaded and the contralateral limb serving as nonloaded control. For the unloading experiment, a second group of mice underwent hindlimb disuse for 3 weeks via tail suspension and the third group of mice served as an age-matched control group for the disuse group and had normal cage activities for 3 weeks. All experimental procedures were approved by Purdue University's Animal Care and Use Committee.

2.2. In vivo tibial loading experiment

Cyclic compressive loads were applied to the left tibia of each mouse with a loading machine (TestBench, TA Instruments) fitted with custom fixtures (Fig. 1A) (Fritton et al., 2005; Main et al., 2014; Yang et al., 2014). The left tibia was maintained in the loading device using a −1 N pre-load and 216 cycles of

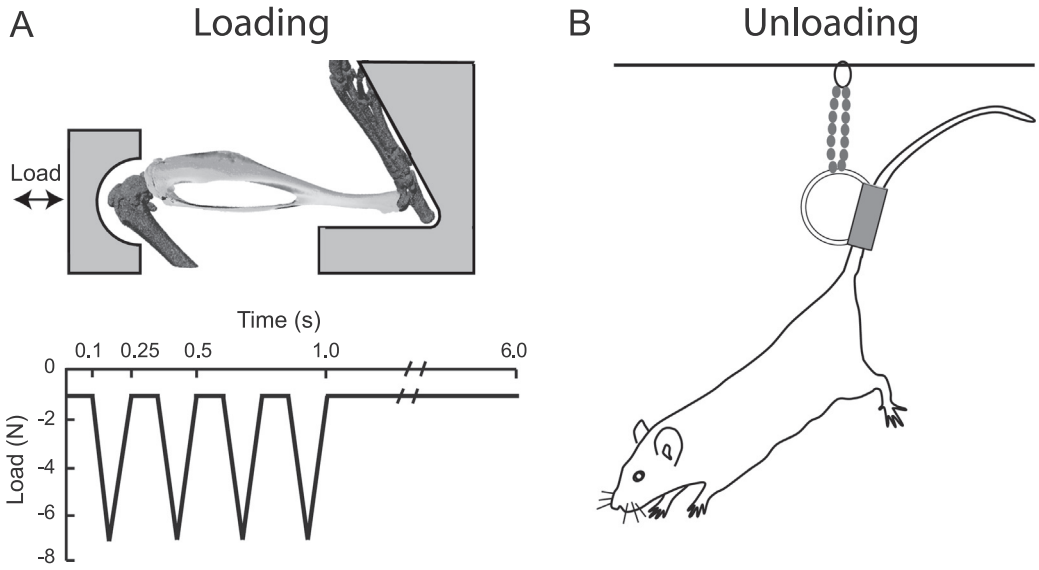

Fig. 1. Setups for the in vivo mouse tibial loading and hindlimb unloading experiments: (A) cyclic compressive loads (−7 N, 4 Hz, 216 cycles) were applied to the mouse tibia through a custom loading device; (B) mice underwent hindlimb disuse via tail suspension.

compressive triangle waveform loads with −7 N peaks were applied at 4 Hz with a 5 s rest interval at −1 N inserted following every fourth load cycle (Fig. 1A) (Willie et al., 2013). Based on our strain gauge measures and finite element modeling performed in a separate group of 16-week-old female C57BL/6 mice, the −7 N peak force would induce peak strains of −2644 με and −2939 με in the proximal metaphyseal cancellous and midshaft cortical bone, respectively (Yang et al., 2014). This compressive load magnitude has been shown to induce anabolic responses in the proximal cancellous and midshaft cortical bone of the tibiae of female C57BL/6 mice of similar age (Sugiyama et al., 2012; Weatherholt et al., 2013). Following 2 weeks of in vivo tibial loading (5 days/week; Monday through Friday), mice were euthanized at 18 weeks of age and tibiae dissected, fixed in 10% neutral buffered formalin for 48hrs, then stored in 70% ethanol at room temperature.

2.3. Hindlimb unloading experiment

For the hindlimb disuse experiments, female 16-week-old mice were individually housed in standard rat cages with a thin metal bar spanning the length of the cage (Fig. 1B). Following one week of normal cage activity acclimation to their cages, the mice were anesthetized (2% isoflurane, 1.0 L/min O2) and the proximal half of the tail taped to a metal key ring using elastic tape. Once the mouse was removed from anesthesia, the key ring was attached to a fishing swivel with ballchain running through its other end and looped around the metal bar near the top of the cage. The ballchain easily slid along the bar and the length of the chain was adjusted so that the hindlimbs were just unable to graze the cage bottom when fully extended. Mice were suspended for 3 weeks and euthanized immediately at the end of the experiment (21 day) at 19 weeks of age. The security of the tail suspension devices was checked 1–2 times per day throughout the experiment. A group of control mice, simultaneously housed in similar cages for 3 weeks, but left unsuspended, acted as age-matched, non-suspended, normal activity controls. After the mice were sacrificed, the tibiae were dissected and stored.

2.4. MicroCT imaging and analysis

For the tibial loading experiment, tibiae from left (loaded) and right (control) limbs of the mice were scanned by microCT (μCT 40, Scanco Medical AG). For the hindlimb unloading experiment, tibiae from right limbs of both the suspended and non-suspended control mice were scanned. Scans were made at an isotropic voxel resolution of 10 μm (55 kVp, 145 mA, 300 ms integration time, no frame averaging). The proximal metaphyseal cancellous and midshaft cortical volume of interests (VOIs) were analyzed (Lynch et al., 2011; Main et al., 2010) (Figs. 2 and 3). Although whole-tibia analyses from previous studies have observed relatively robust mechanoadaptive responses along ~10–60% of the tibia from its proximal end (Javaheri et al., 2018; Carriero et al., 2018; De Souza et al., 2017; Galea et al.,2015; Yang et al., 2017), the midshaft was chosen here because it is a common location where strain gauging is performed and load-strain relations are established. It is also a common volume of interest for examining cortical bone adaptation in the tibial loading model (Sugiyama et al., 2012; Weatherholt et al., 2013; Holguin et al., 2014; Lynch et al., 2011; Main et al., 2014; Willie et al., 2013; Berman et al., 2015; Yang et al., 2017). Thresholds of 0.41 and 0.34 g HA/cm^3 were used to segment the proximal cancellous and midshaft cortical bone, respectively, for all tibiae from the loading experiment. Thresholds of 0.29 and 0.28 g HA/cm^3 were used to segment the proximal cancellous and midshaft cortical bone, respectively, for the all tibiae from the disuse experiment. The thresholds were determined according to previous methods (Main et al., 2010; Melville et al., 2013; Willie et al., 2013) and confirmed by visual inspection. Midshaft cortical parameters including cortical area (Ct.Ar), total area (Tt.Ar), marrow area (Ma.Ar), maximum and minimum moments of inertia (Imax and Imin) as well as metaphyseal cancellous parameters including bone volume fraction (BV/TV), trabecular thickness (Tb.Th), trabecular separation (Tb.Sp) and trabecular number (Tb.N) were measured (Bouxsein et al. 2010).

2.5. MicroCT-based finite element analysis

MicroCT-based FE analysis was performed to determine the changes in tissue-level mechanical environments as a result of loading or unloading, particularly in the proximal metaphyseal cancellous and midshaft cortical VOIs of the tibia. The FE approach has been developed and validated previously via strain gauge measurement and comprehensive sensitivity analyses (Yang et al., 2014). Briefly, tibial FE mesh models consisting of tetrahedral elements were bulit from microCT images. Heterogeneous isotropic bone tissue material properties were assigned to the FE models (Yang et al., 2010). All bone elements were assigned a Poisson's ratio of 0.3 (Silva et al., 2005). In order to make direct comparisons in strain magnitude and distribution between control and loaded/unloaded tibiae, the same loading and boundary conditions were applied to all tibiae, replicating the in vivo tibial compressive loading configuration (Yang et al., 2014). Linear elastic FE analysis was performed in Abaqus 6.13.3 (Simulia). A total of 33 FE models were created, including 14 FE models for the tibial loading experiment (7 loaded and 7 control) and 19 FE models for the hindlimb unloading experiment (9 unloaded and 10 control). All tibiae that were evaluated by microCT were then used for FE modeling.

2.6. Data analysis

The maximum and minimum principal and longitudinal strains were calculated for each bone element of the proximal metaphyseal cancellous and midshaft cortical VOIs as well as cortical bone at a distance 37% of the tibia's length from its proximal end. To explore how load or disuse affected the overall strain distribution (occurrence of different strain magnitudes) in the post-adapted bones we examined the frequency distributions of strain magnitudes throughout the cortical and canellous VOIs (Ozcivici et al., 2007; Razi et al., 2015b). To determine how load or disuse altered the overall strain magnitudes, we ranked the maximum principal strain, minimum principal strain or longitudinal strain values and analyzed and compared their percentiles (5th, 10th, 25th, 50th, 75th, 90th and 95th) between loaded/unloaded and control cortical or cancellous VOIs (Ozcivici et al., 2007). The strain percentile (e.g. 95th) represents the strain value for cutting off the relevant percentage (e.g. top 5%) of bone elements (Yang et al., 2014; Yang et al., 2012). The effect of loading was examined by paired *t*-tests and the effect of unloading was assessed by unpaired *t*-tests. Relationships between strain magnitudes and each cancellous or cortical microCT parameter were determined by linear regression analyses. All statistical analyses were performed in SPSS (IBM SPSS 22.0) and significance was set as $p < 0.05$.

3. Results

3.1. Bone mass changes with loading/unloading

Loading or unloading significantly altered cancellous and cortical bone mass and the change in bone mass was more pronounced in the proximal metaphyseal cancellous than midshaft cortical bone of the tibia. BV/TV and Tb.Th of the metaphyseal cancellous

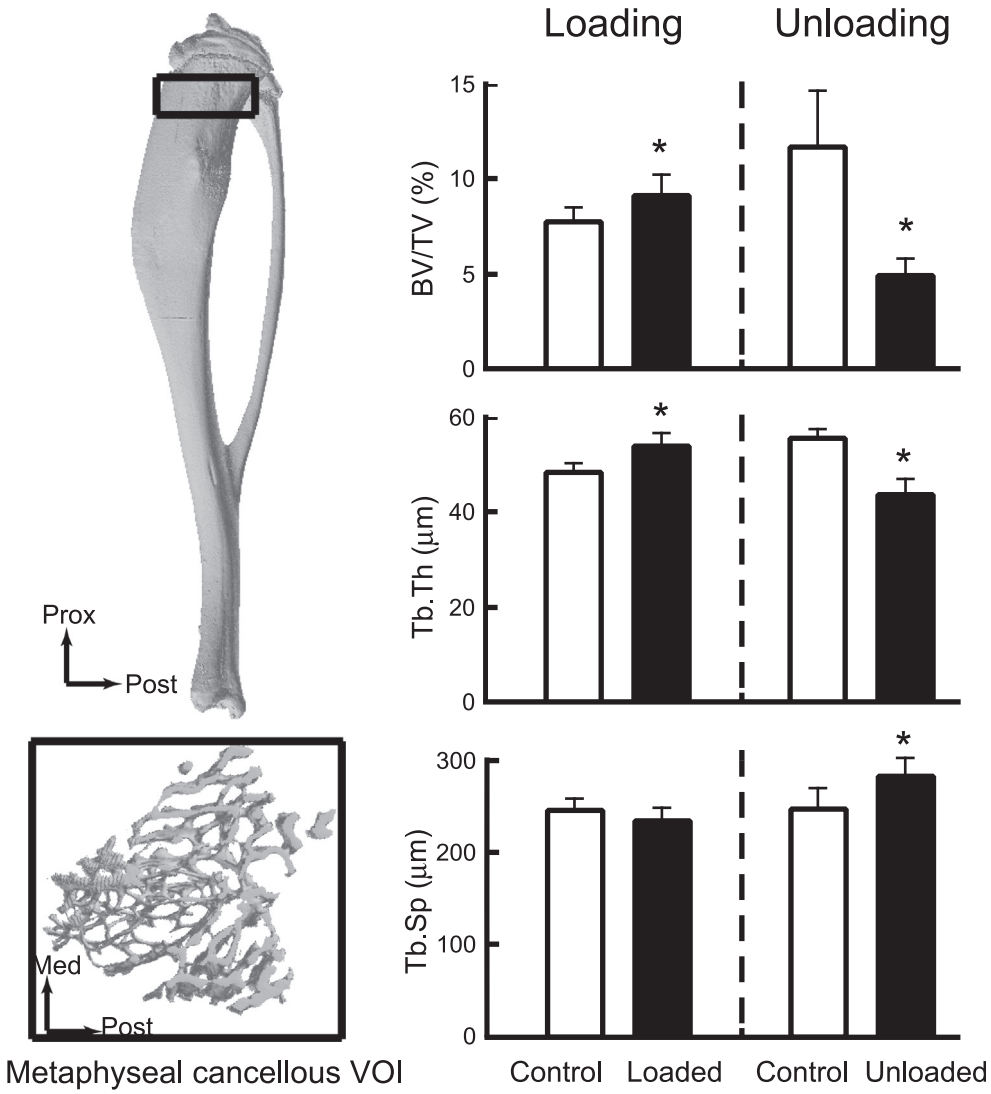

Fig. 2. Changes in microCT-measured parameters of the proximal metaphyseal cancellous bone of the tibiae with applied compressive loading or hindlimb unloading. The proximal metaphyseal cancellous volume of interest (VOI) began approximately 0.5 mm distal to the proximal growth plate, excluding the primary spongiosa and cortical shell, and extended 5% of the total tibial length. *$p < 0.05$ (paired *t*-test for control vs. loaded limbs or unpaired *t*-test for control vs. unloaded tibiae). Bars: mean + SD.

bone increased by 18% and 12% with applied load, respectively (Fig. 2), while Ct.Ar and Tt.Ar of the tibial midshaft increased by 6% and 2% with loading, respectively (Fig. 3; Table A1 in Appendix). Loading had no effect on Tb.N and Tb.Sp. There was a non-significant decrease of 3% in Ma.Ar ($p = 0.25$; Table A1 in Appendix), indicating a periosteal expansion with loading. In the proximal cancellous bone, unloading led to a marked reduction of BV/TV (-58%) and was associated with decreased Tb.Th (−22%), reduced Tb.N (−15%) and increased Tb.Sp (15%) (Fig. 2). In the midshaft, unloading led to a decrease of 12% in Ct.Ar and an increase of 24% in Ma.Ar without significant changes in Tt.Ar (Fig. 3; Table A1 in Appendix), indicating an endocortical erosion with unloading. Loading or unloading did not affect Imax and Imin (Fig. 3).

3.2. Altered tissue-level mechanical environments with loading/unloading

In the longitudinal loading direction, there was a shift in the metaphyseal cancellous VOI toward lower strains for the loaded relative to control tibiae (Fig. 4). The percentage of bone elements in the cancellous VOI was significantly decreased in the loaded tibia relative to the control limb in the longitudinal strain range from −2000 to −1500 με (12% vs. 9%), while the percentage of elements in the longitudinal strain range from −1200 to −300 με was significantly increased (38% vs. 48%) (Fig. 4). In addition, there was a load-induced decrease in the percentage of elements in tension (200 to 894 με) in the loaded relative to the control tibia (13% vs. 9%), which may correspond to an increased percentage of low compression elements due to the increased bone mass (Fig. 4). In the midshaft, there was a significant load-induced decrease in the percentage of elements at strain values of −3400 and 2900 με (Fig. 5). A significant increase in the percentage of element was observed at strain values around −1400 με. There were no significant differences in the proportion of elements between control and loaded tibiae for the rest of the strain ranges (Fig. 5). The unloading-induced alteration of the strain distributions in both cancellous and cortical VOIs was opposite that for the loading (Figs. 4 and 5). The percentage of high strain elements increased and the percentage of low strain elements decreased following unloading (Figs. 4 and 5).

Consistent with the loading- or unloading-induced alterations in the strain distribution, the longitudinal strain levels were generally reduced with loading and increased with unloading (Table 1).

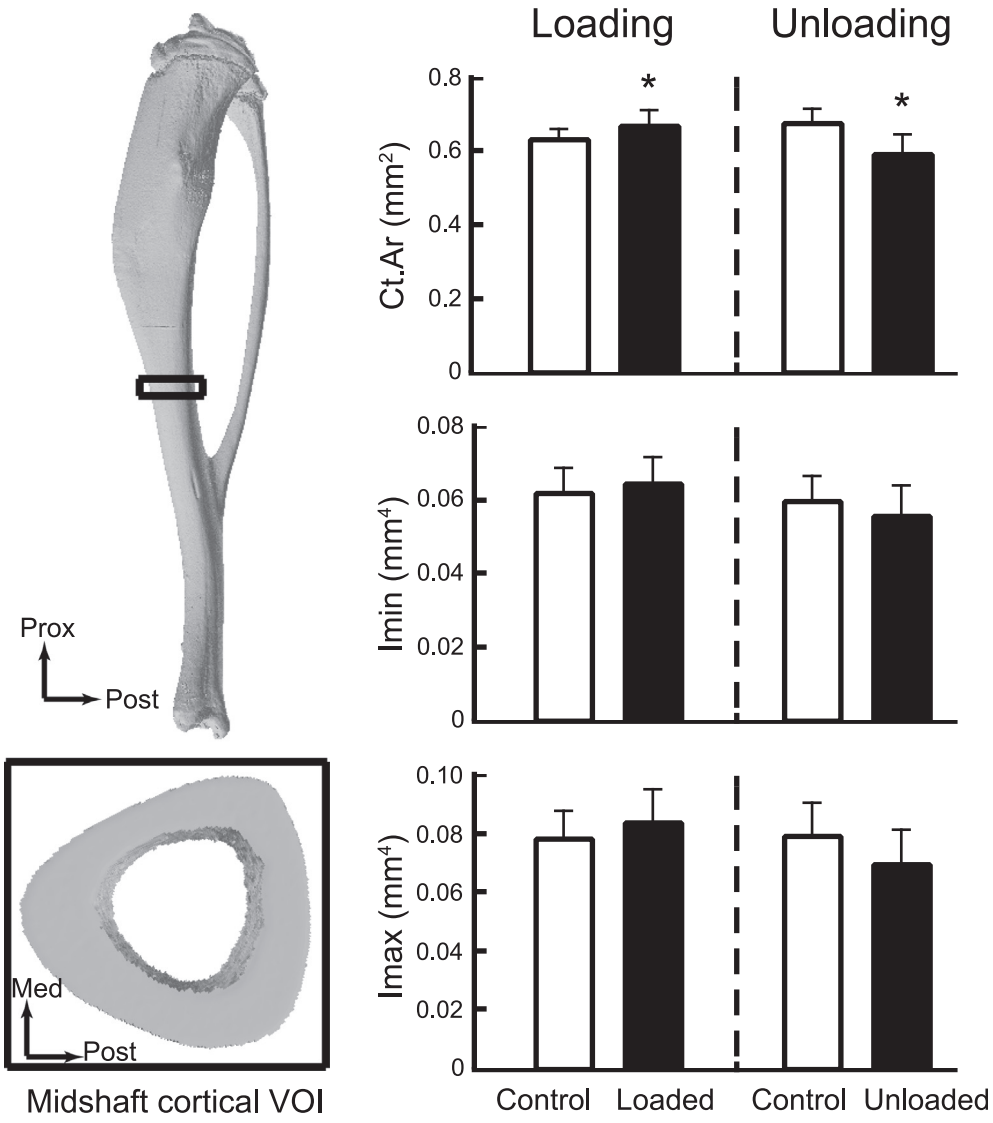

Fig. 3. Changes in microCT-measured parameters of the midshaft cortical bone of the tibiae with applied compressive loading or hindlimb unloading. The midshaft cortical VOI was centered at the middle of the tibia and spanned a total of 2.5% of the total tibial length. *$p < 0.05$ (paired *t*-test for control vs. loaded tibiae or unpaired *t*-test for control vs. unloaded tibiae). Bars: mean + SD.

Interestingly, there was no significant change in the maximum or minimum principal strain magnitudes as a result of loading for either the proximal cancellous or midshaft cortical VOIs (Figs. 6 and 7). Unloading had a greater effect on the relative increases in strain magnitudes in the metaphyseal cancellous tissues than the midshaft cortical tissues. Unloading resulted in increases in maximum and minimum principal strains at 50th (68% and 78%, respectively), 75th (106% and 78%), 90th (128% and 132%) and 95th percentiles (137% and 165%) for the metaphyseal cancellous bone (Fig. 6). The unloaded tibia had increased maximum and minimum principal strains in the midshaft cortical bone at the 25th (28% and 24%), 50th (36% and 20%), 75th (22% and 35%), 90th (21% and 33%) and 95th percentiles (20% and 31%) relative to the control (Fig. 7). The loading- or unloading-induced alterations in strain magnitude and distribution at 37% cortical bone were similar to 50% midshaft (see Appendix).

3.3. Relationship between bone mass and tissue-level strains

Bone mass was a good predictor of bone tissue strains for the midshaft cortical bone but not for the metaphyseal cancellous bone. For loading or unloading experiments, there were moderate or strong correlations between cortical parameters and the magnitudes of the percentiles for maximum or minimum principal strains in the tibial midshaft (Table 2). In contrast, very poor or no correlations were found for the metaphyseal cancellous bone between trabecular parameters and maximum or minimum principal strains (Table 3).

4. Discussion

The goal of this study was to determine the adaptive changes in tissue-level mechanical environments of metaphyseal cancellous and midshaft cortical bone of the tibia in response to in vivo loading or disuse. We found that loading or unloading significantly altered cancellous and cortical bone mass and the changes in bone mass seemed more pronounced in the metaphyseal cancellous than midshaft cortical bone of the tibia. The loading- or unloading-induced changes in cancellous and cortical bone mass were accompanied by altered micromechanical environments when the tibiae were virtually loaded in compression. Loading led to an increased percentage of bone tissue experiencing lower

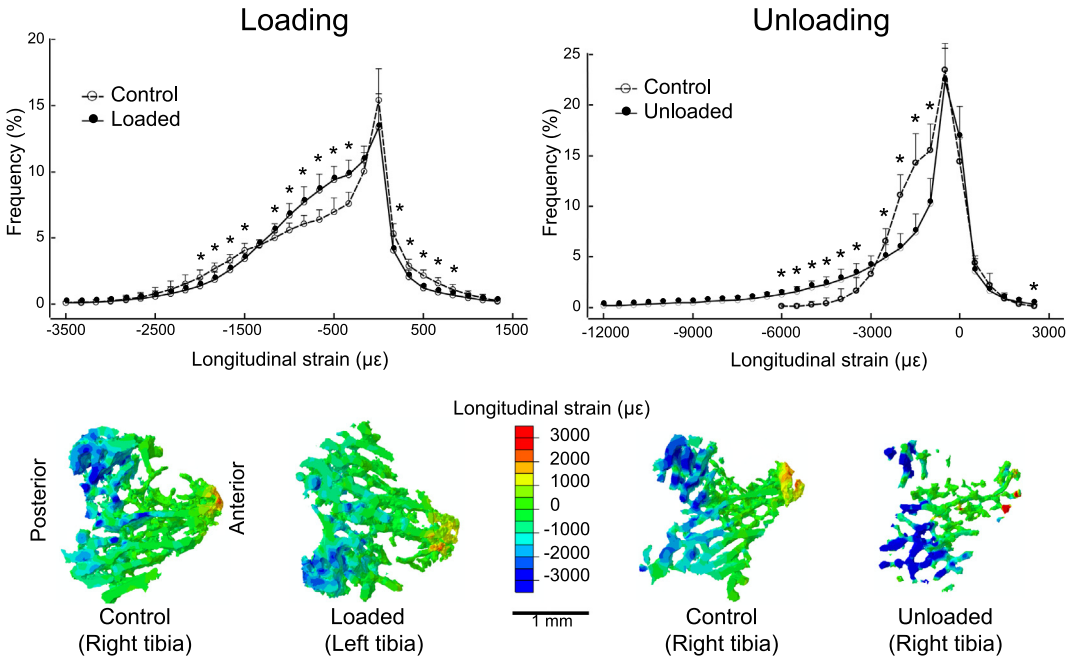

Fig. 4. Changes in longitudinal strain distribution of the proximal metaphyseal cancellous bone of the tibiae with applied loading or hindlimb unloading when the tibiae were virtually loaded in axial compression of −7 N. *p < 0.05 (paired *t*-test for control vs. loaded tibiae or unpaired *t*-test for control vs. unloading tibiae). Bars: mean + SD. The area under each curve is equal to 100%.

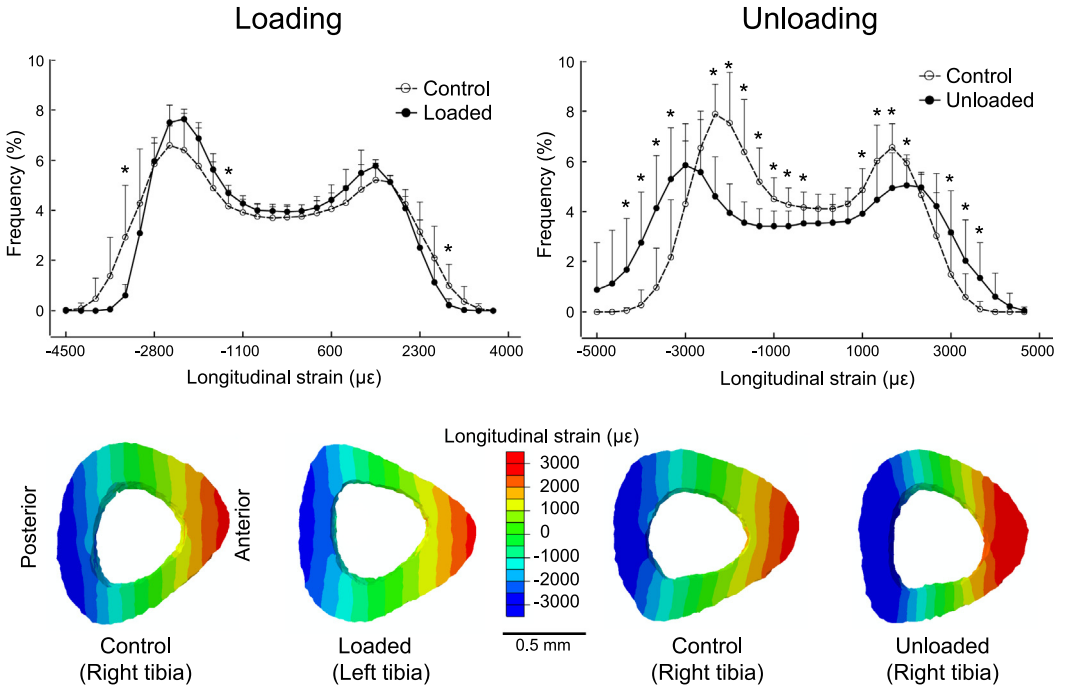

Fig. 5. Changes in longitudinal strain distribution of the midshaft cortical bone of the tibiae with applied loading or hindlimb unloading when the tibiae were virtually loaded in axial compression of −7 N. *p < 0.05 (paired *t*-test for control vs. loaded tibiae or unpaired *t*-test for control vs. unloaded tibiae). Bars: mean + SD. The area under each curve is equal to 100%.

strains in the longitudinal loading direction relative to the non-loaded limb. Unloading caused an opposite effect where a greater percentage of the cancellous volume experienced greater strains compared to age-matched controls. Interestingly, the maximum or minimum principal strains of cortical and cancellous bone of the tibia were not affected by loading, indicating that the load-adapted tissue-level mechanical benefits were gained primarily in the primary loading direction. In addition, regression analyses demonstrated that bone mass was a good predictor of bone tissue strains for the midshaft cortical bone but not for the metaphyseal

Table 1
Longitudinal strains (με) in the metaphyseal cancellous and midshaft cortical bone of the control and loaded/unloaded tibiae when virtually subjected to a compression load of −7 N.

Longitudinal strain	Loading			Unloading		
	Control (n = 7)	Loaded (n = 7)	Diff (%)	Control (n = 9)	Unloaded (n = 10)	Diff (%)
Metaphyseal cancellous bone				−2698 ± 551	−6999 ± 1888	**159**
5th percentile	−2062 ± 292	−1916 ± 359	−7	−2258 ± 442	−5051 ± 1370	**124**
10th percentile	−1735 ± 235	−1570 ± 269	−10	−1494 ± 162	−2480 ± 639	**66**
25th percentile	−1135 ± 137	−1028 ± 128	−9	−625 ± 136	−651 ± 328	4
50th percentile	−454 ± 89	−508 ± 89	12	−36 ± 38	−10 ± 35	−72
75th percentile	−24 ± 22	−102 ± 55	**324**	381 ± 141	374 ± 214	−2
90th percentile	242 ± 59	96 ± 59	**−61**	807 ± 250	956 ± 544	18
95th percentile	557 ± 98	356 ± 122	**−36**			
Midshaft cortical bone						
5th percentile	−2899 ± 329	−2630 ± 100	**−9**	−3183 ± 402	−4185 ± 776	**31**
10th percentile	−2656 ± 302	−2416 ± 96	−9	−2917 ± 365	−3890 ± 733	**33**
25th percentile	−2056 ± 236	−1888 ± 92	−8	−2272 ± 285	−3057 ± 582	**35**
50th percentile	−569 ± 51	−558 ± 49	−2	−613 ± 69	−689 ± 91	12
75th percentile	1182 ± 150	1075 ± 90	−9	1393 ± 219	1709 ± 355	**23**
90th percentile	1975 ± 236	1802 ± 148	−9	2200 ± 312	2672 ± 492	**21**
95th percentile	2300 ± 278	2097 ± 170	−9	2544 ± 348	3070 ± 541	**21**

Data are presented as mean ± SD.
Bold indicates $p < 0.05$ by paired or unpaired *t*-tests.

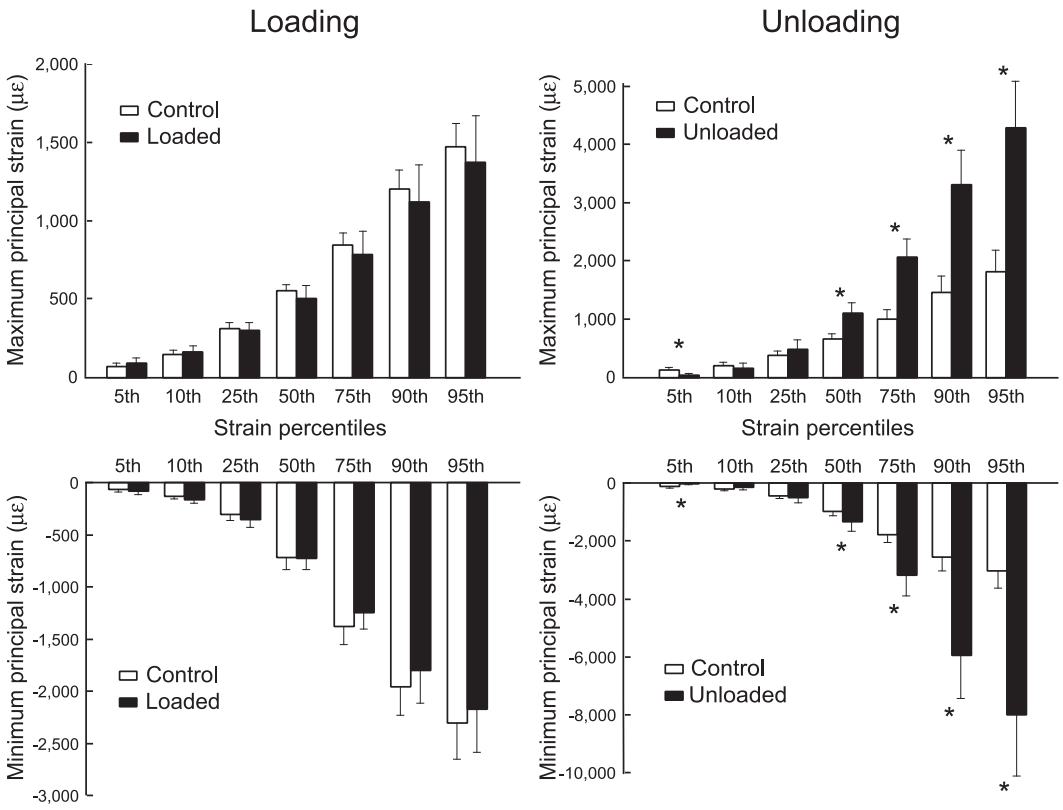

Fig. 6. Loading- or unloading-induced changes in the magnitudes of the maximum and minimum principal strains of the proximal metaphyseal cancellous bone tissues. *$p < 0.05$ by paired or unpaired *t*-tests. Bars: mean + SD.

cancellous bone. In summary, loading-induced biomechanical benefits for cancellous and cortical bone are received primarily in the direction of force application and bone mass may not relate to micromechanics of cancellous bone.

Our results show that cancellous tissues are more sensitive to changes in external mechanical environment compared to cortical tissues. With applied two-week tibial loading, the increase in bone volume of the metaphyseal cancellous bone (BV/TV) was greater than that of the midshaft cortical bone (Ct.Ar). This result is consistent with previous observations of tibial loading studies (Holguin et al., 2014; Main et al., 2014; Sugiyama et al., 2012; Willie et al., 2013; Yang et al., 2017b). Our current and previous studies show that the peak and average strains are significantly lower in the proximal cancellous bone than in the midshaft cortical bone in this tibial loading model (Yang et al., 2014), suggesting that the greater response of the proximal cancellous bone relative to midshaft cortical bone to loading is not directly related with tissue strain levels. Also, the different degrees of response to loading between cortical and cancellous tissues are not specific to the tibial loading model as our unloading experiment demonstrated that three-week

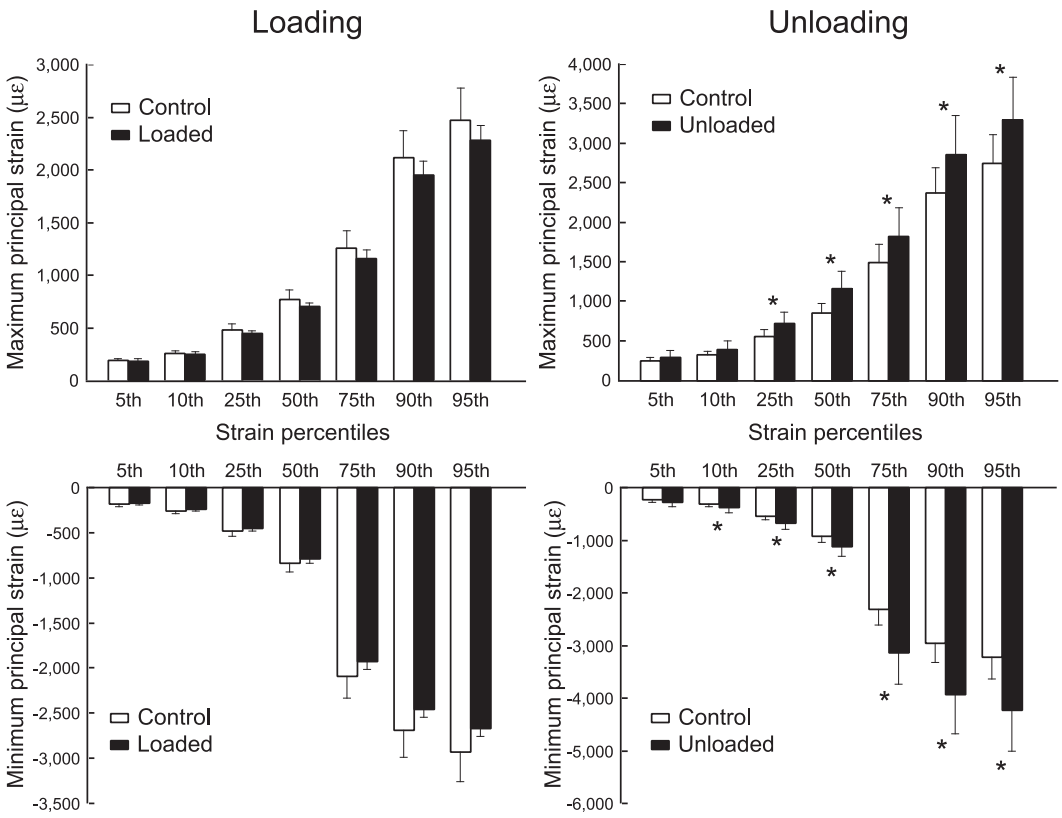

Fig. 7. Loading- or unloading-induced changes in the magnitudes of the maximum and minimum principal strains of the midshaft cortical bone tissues. *p < 0.05 by paired or unpaired *t*-tests. Bars: mean + SD.

Table 2
Correlation (R squares) between percentiles of principal strains and microCT parameters of the midshaft cortical bone.

Strain Percentiles	Loading								Unloading							
	Control				Loaded				Control				Unloaded			
	Ct.Ar	Imin	Imax	Ma.Ar	Ct.Ar	Imin	Imax	Ma.Ar	Ct.Ar	Imin	Imax	Ma.Ar	Ct.Ar	Imin	Imax	Ma.Ar
Maximum Principal Strain																
5th	**0.61**	**0.64**	**0.65**	0.50	**0.70**	**0.88**	**0.84**	**0.67**	**0.78**	**0.65**	**0.75**	0.29	**0.86**	**0.80**	**0.68**	0.12
10th	**0.76**	**0.80**	**0.81**	**0.69**	**0.75**	**0.87**	**0.89**	**0.64**	**0.75**	**0.61**	**0.71**	0.28	**0.91**	**0.84**	**0.75**	0.14
25th	**0.65**	**0.73**	**0.77**	**0.75**	**0.89**	0.49	**0.63**	0.37	**0.78**	**0.48**	**0.69**	0.15	**0.91**	**0.84**	**0.79**	0.16
50th	**0.65**	**0.73**	**0.79**	**0.77**	0.40	0.07	0.20	0.00	**0.67**	0.39	**0.62**	0.15	**0.87**	**0.75**	**0.73**	0.10
75th	**0.69**	**0.73**	**0.87**	**0.78**	**0.67**	0.23	0.33	0.10	**0.79**	**0.44**	**0.68**	0.11	**0.78**	**0.76**	**0.77**	0.20
90th	**0.70**	**0.71**	**0.82**	**0.70**	**0.64**	0.21	0.31	0.15	**0.77**	**0.49**	**0.68**	0.16	**0.73**	**0.71**	**0.73**	0.20
95th	**0.71**	**0.69**	**0.80**	**0.67**	**0.66**	0.22	0.34	0.17	**0.76**	**0.49**	**0.66**	0.16	**0.72**	**0.70**	**0.72**	0.19
Minimum Principal Strain																
5th	0.56	**0.68**	**0.75**	**0.72**	**0.82**	**0.77**	**0.82**	**0.61**	**0.69**	**0.66**	**0.74**	0.39	**0.86**	**0.80**	**0.72**	0.14
10th	**0.61**	**0.69**	**0.85**	**0.81**	**0.89**	0.53	**0.67**	0.40	**0.72**	**0.62**	**0.74**	0.32	**0.87**	**0.80**	**0.75**	0.14
25th	**0.60**	**0.66**	**0.80**	**0.77**	0.47	0.08	0.18	0.05	**0.75**	0.41	**0.62**	0.09	**0.76**	**0.74**	**0.75**	0.20
50th	**0.64**	**0.64**	**0.78**	**0.69**	**0.79**	0.37	0.52	0.30	**0.74**	**0.51**	**0.65**	0.17	**0.75**	**0.74**	**0.75**	0.21
75th	**0.61**	**0.66**	**0.78**	**0.74**	0.50	0.19	0.38	0.03	**0.64**	0.32	**0.53**	0.09	**0.86**	**0.74**	**0.69**	0.08
90th	**0.65**	**0.71**	**0.79**	**0.74**	**0.77**	0.47	**0.67**	0.21	**0.69**	0.43	**0.64**	0.17	**0.86**	**0.74**	**0.70**	0.09
95th	**0.67**	**0.71**	**0.79**	**0.72**	**0.87**	**0.65**	**0.80**	0.38	**0.70**	**0.46**	**0.66**	0.20	**0.86**	**0.76**	**0.71**	0.11

Data are presented as R^2 values. Ct.Ar: cortical area. Imin and Imax: minimum and maximum moments of inertia. Ma.Ar: marrow area.
Bold indicates p < 0.05.

hindlimb unloading led to a reduction of 58% in cancellous bone volume fraction vs. a decrease of only 12% in midshaft cortical area. Our results together with others imply that cancellous tissues are more sensitive to the changes in mechanical environments than cortical bone. Riggs et al. reported that women experienced 37% and men experienced 42% of their total lifetime trabecular bone loss before the age of 50, compared to 6% and 15%, respectively for cortical bone (Riggs et al., 2008). Whether or not the different sensitivities between cortical and cancellous bone tissues to the changes in mechanical environments could contribute to the difference between cortical and cancellous bone loss remains a question and may require further research.

Our results indicate that load-induced micromechanical outcomes occur mainly in the direction of force application for the tibial loading model. Post-adaptive reduction in strain in the longitudinal loading direction was also observed on diaphyseal surfaces of the tibia based on DIC measurements (Sztefek et al., 2010). Since loading can enhance bone mass and unloading can

Table 3
Correlation (R squares) between percentiles of principal strains and microCT parameters of the metaphyseal cancellous bone.

Strain Percentiles	Loading								Unloading							
	Control				Loaded				Control				Unloaded			
	BV/TV	Tb.Th	Tb.Sp	Tb.N	BV/TV	Tb.Th	Tb.Sp	Tb.N	BV/TV	Tb.Th	Tb.Sp	Tb.N	BV/TV	Tb.Th	Tb.Sp	Tb.N
Maximum Principal Strain																
5th	0.03	0.17	0.15	0.08	0.00	0.45	**0.72**	0.47	0.26	0.00	0.06	0.17	0.01	0.14	0.23	**0.45**
10th	0.03	0.34	0.12	0.08	0.09	**0.71**	0.41	0.20	0.21	0.01	0.02	0.13	0.03	0.22	0.09	0.23
25th	0.04	0.40	0.11	0.08	0.43	**0.86**	0.10	0.00	0.13	0.04	0.00	0.08	0.05	0.21	0.02	0.16
50th	0.11	0.32	0.02	0.01	0.25	**0.78**	0.08	0.01	0.01	0.38	0.10	0.00	0.00	0.00	0.10	0.02
75th	0.29	0.23	0.01	0.03	0.07	0.56	0.06	0.05	0.12	**0.61**	0.27	0.09	0.14	0.34	0.29	0.00
90th	0.28	0.27	0.00	0.02	0.05	0.49	0.05	0.06	0.19	**0.67**	0.34	0.14	**0.42**	**0.63**	0.19	0.01
95th	0.29	0.29	0.00	0.03	0.05	0.52	0.06	0.06	0.20	**0.70**	0.33	0.14	**0.53**	**0.59**	0.08	0.05
Minimum Principal Strain																
5th	0.01	0.11	0.27	0.16	0.00	0.48	0.52	0.47	0.24	0.00	0.04	0.15	0.01	0.16	0.26	**0.47**
10th	0.05	0.15	0.11	0.05	0.10	**0.66**	0.19	0.17	0.21	0.00	0.02	0.10	0.03	0.20	0.07	0.24
25th	0.25	0.19	0.00	0.02	0.12	0.54	0.03	0.10	0.17	0.01	0.00	0.06	0.08	0.22	0.00	0.11
50th	0.32	0.34	0.03	0.06	0.10	0.52	0.00	0.08	0.11	0.01	0.00	0.01	0.19	0.05	0.11	0.01
75th	0.34	0.20	0.11	0.13	0.03	0.41	0.00	0.09	0.03	0.25	0.25	0.13	0.01	0.22	**0.60**	0.24
90th	0.46	0.13	0.20	0.24	0.00	0.32	0.00	0.13	0.25	**0.60**	0.44	0.29	0.21	**0.65**	0.32	0.03
95th	0.46	0.13	0.20	0.24	0.00	0.32	0.00	0.13	0.25	**0.60**	0.44	0.29	0.21	**0.65**	0.32	0.03

Data are presented as R^2 values. BV/TV: bone volume fracture. Tb.Th: trabecular thickness. Tb.Sp: trabecular separation. Tb.N: trabecular number.
Bold indicates $p < 0.05$.

result in bone loss, one would expect that tissue-level strains would be reduced following loading and increased with unloading. Interestingly, we find that either maximum or minimum principal strain magnitudes that may be related to risk of tissue failure (Yang et al., 2012) are not significantly affected by loading. These findings suggest that mechanical loading could lead to an increased bone mass that might not be associated with an general improvement of biomechanical behavior of bone tissue, but is instead a specific response to load applied in a specific consistent direction. To this end, we see an alteration in the proportion of cancellous bone elements from high to low strain ranges in the longitudinal loading direction, indicating the overall level of the longitudinal strains are reduced due to loading. Since the effect of unloading is not direction-specific the alterations in maximum or minimum principal strains are similar to the longitudinal strains.

We find no correlation between bone mass and tissue-level strains for the proximal cancellous bone, suggesting that cancellous bone mass, itself, cannot predict the micromechanics of cancellous bone. The association between bone mass and tissue-level strains in the midshaft cortical bone of the tibia can be explained by beam theory. The midshaft undergoes a combined bending and compression loading when the tibia is loaded axially in compression in vivo. Thus, the distribution and magnitude of tissue strains depend on the geometry (or mass) of the midshaft's cross-section. However, for the proximal cancellous bone, the mechanical behavior of the cancellous tissues depends largely on its complex microarchitecture (Goff et al., 2015; Morgan et al., 2004) and may not be explained simply by one or multiple morphological parameters. Therefore, computational approaches like finite element analysis might be useful to evaluate the effects of mechanical stimuli on biomechanics of bone tissues, particularly for cancellous bone, as relatively simple measures of bone volume may not be indicative of risk for cancellous bone failure.

There was a disparity in experimental length between the loading and unloading experiments. For the unloading experiment, we did not see a significant disuse response at 2 weeks of hindlimb suspension in a preliminary study ($\Delta BV/TV = -8.5\%$, $p = 0.06$, $n = 10$/group) and therefore decided to pursue 3 weeks of hindlimb unloading. For the loading experiment, the two-week loading term was chosen since it has been commonly used for this tibial loading model in previous studies (Holguin et al., 2014; Lynch et al., 2011; Main et al., 2014; Willie et al., 2013; Berman et al., 2015; Yang et al., 2017). It remains unclear if another week of loading would enhance the bone formation described here and future studies may be required to address this issue. However, our goal was not to compare head-to-head the amount of bone lost or gained by a specific period of unloading or loading. The primary goal of this study was to examine how the micromechanical environments of cancellous and cortical tissues alter following the adaptive changes in their bone mass resulting from loading or unloading, separately — both loading and unloading protocols used here induced significant changes in cortical and cancellous bone mass, as was required for our analysis.

In summary, we find in the tibial loading model that cancellous tissues are more sensitive to mechanical environments compared to cortical tissues; loading-induced micromechanical benefits for cancellous bone are received primarily in the direction of load application and cancellous bone mass may not be related to the micromechanics of cancellous bone.

Acknowledgements

This work was supported by the National Science Foundation (NSF CMMI-1463523) and the National Natural Science Foundation of China (11702008, 11832003). Support Plan for High-level Faculties in Beijing Municipal Universities (CIT&TCD201804011) and Beijing Excellent Talents Funding (2017000020124G277) are also acknowledged. Dr. Dafang Chen helped in conducting the animal studies and Grema Adam helped in performing microCT analysis.

Conflict of Interest

The authors have no conflict of interest.

Appendix A. Supplementary material

Supplementary data to this article can be found online at https://doi.org/10.1016/j.jbiomech.2019.04.021.

References

Baumann, A.P., Aref, M.W., Turnbull, T.L., Robling, A.G., Niebur, G.L., Allen, M.R., Roeder, R.K., 2015. Development of an in vivo rabbit ulnar loading model. Bone 75, 55–61.

Berman, A.G., Clauser, C.A., Wunderlin, C., Hammond, M.A., Wallace, J.M., 2015. Structural and mechanical improvements to bone are strain dependent with axial compression of the Tibia in female C57BL/6 Mice. PloS One 10, e0130504.
Bertram, J.E., Swartz, S.M., 1991. The 'law of bone transformation': a case of crying Wolff? Biol. Rev. Camb. Philos. Soc. 66, 245–273.
Birkhold, A.I., Razi, H., Duda, G.N., Weinkamer, R., Checa, S., Willie, B.M., 2014. The influence of age on adaptive bone formation and bone resorption. Biomaterials 35, 9290–9301.
Birkhold, A.I., Razi, H., Duda, G.N., Checa, S., Willie, B.M., 2017. Tomography-based quantification of regional differences in cortical bone surface remodeling and mechano-response. Calcif. Tissue Int. 100, 255–270.
Bouxsein, M.L., Boyd, S.K., Christiansen, B.A., Guldberg, R.E., Jepsen, K.J., Muller, R., 2010. Guidelines for assessment of bone microstructure in rodents using micro-computed tomography. J. Bone Miner. Res. 25, 1468–1486.
Carriero, A., Abela, L., Pitsillides, A.A., Shefelbine, S.J., 2014. Ex vivo determination of bone tissue strains for an in vivo mouse tibial loading model. J. Biomech. 47, 2490–2497.
Carriero, A., Pereira, A.F., Wilson, A.J., Castagno, S., Javaheri, B., Pitsillides, A.A., Marenzana, M., Shefelbine, S.J., 2018. Spatial relationship between bone formation and mechanical stimulus within cortical bone: Combining 3D fluorochrome mapping and poroelastic finite element modelling. Bone Rep. 8, 72–80.
De Souza, R., Javaheri, B., Collinson, R.S., Chenu, C., Shefelbine, S.J., Lee, P.D., Pitsillides, A.A., 2017. Prolonging disuse in aged mice amplifies cortical but not trabecular bones' response to mechanical loading. J. Musculoskelet. Neuronal. Interact. 17, 218–225.
De Souza, R.L., Matsuura, M., Eckstein, F., Rawlinson, S.C., Lanyon, L.E., Pitsillides, A. A., 2005. Non-invasive axial loading of mouse tibiae increases cortical bone formation and modifies trabecular organization: a new model to study cortical and cancellous compartments in a single loaded element. Bone 37, 810–818.
Fritton, J.C., Myers, E.R., Wright, T.M., van der Meulen, M.C., 2005. Loading induces site-specific increases in mineral content assessed by microcomputed tomography of the mouse tibia. Bone 36, 1030–1038.
Galea, G.L., Hannuna, S., Meakin, L.B., Delisser, P.J., Lanyon, L.E., Price, J.S., 2015. Quantification of alterations in cortical bone geometry using site specificity software in mouse models of aging and the responses to ovariectomy and altered loading. Front. Endocrinol. (Lausanne). 6, 52.
Gerbaix, M., Gnyubkin, V., Farlay, D., Olivier, C., Ammann, P., Courbon, G., Laroche, N., Genthial, R., Follet, H., Peyrin, F., Shenkman, B., Gauquelin-Koch, G., Vico, L., 2017. One-month spaceflight compromises the bone microstructure, tissue-level mechanical properties, osteocyte survival and lacunae volume in mature mice skeletons. Sci. Rep. 7, 2659.
Goff, M.G., Lambers, F.M., Sorna, R.M., Keaveny, T.M., Hernandez, C.J., 2015. Finite element models predict the location of microdamage in cancellous bone following uniaxial loading. J. Biomech. 48, 4142–4148.
Gross, T.S., Srinivasan, S., Liu, C.C., Clemens, T.L., Bain, S.D., 2002. Noninvasive loading of the murine tibia: an in vivo model for the study of mechanotransduction. J. Bone Miner. Res. 17, 493–501.
Haapasalo, H., Kontulainen, S., Sievanen, H., Kannus, P., Jarvinen, M., Vuori, I., 2000. Exercise-induced bone gain is due to enlargement in bone size without a change in volumetric bone density: a peripheral quantitative computed tomography study of the upper arms of male tennis players. Bone 27, 351–357.
Holguin, N., Brodt, M.D., Sanchez, M.E., Silva, M.J., 2014. Aging diminishes lamellar and woven bone formation induced by tibial compression in adult C57BL/6. Bone 65, 83–91.
Javaheri, B., Carriero, A., Wood, M., De Souza, R., Lee, P.D., Shefelbine, S., Pitsillides, A. A., 2018. Transient peak-strain matching partially recovers the age-impaired mechanoadaptive cortical bone response. Sci Rep. 8, 6636.
Lambers, F.M., Kuhn, G., Weigt, C., Koch, K.M., Schulte, F.A., Muller, R., 2015. Bone adaptation to cyclic loading in murine caudal vertebrae is maintained with age and directly correlated to the local micromechanical environment. J. Biomech. 48, 1179–1187.
Lanyon, L.E., Rubin, C.T., 1984. Static vs dynamic loads as an influence on bone remodelling. J. Biomech. 17, 897–905.
Lynch, M.E., Main, R.P., Xu, Q., Schmicker, T.L., Schaffler, M.B., Wright, T.M., van der Meulen, M.C., 2011. Tibial compression is anabolic in the adult mouse skeleton despite reduced responsiveness with aging. Bone 49, 439–446.
Lynch, M.E., Main, R.P., Xu, Q., Walsh, D.J., Schaffler, M.B., Wright, T.M., van der Meulen, M.C., 2010. Cancellous bone adaptation to tibial compression is not sex dependent in growing mice. J. Appl. Physiol. 109, 685–691.
Main, R.P., Lynch, M.E., van der Meulen, M.C., 2010. In vivo tibial stiffness is maintained by whole bone morphology and cross-sectional geometry in growing female mice. J. Biomech. 43, 2689–2694.
Main, R.P., Lynch, M.E., van der Meulen, M.C., 2014. Load-induced changes in bone stiffness and cancellous and cortical bone mass following tibial compression diminish with age in female mice. J. Exp. Biol. 217, 1775–1783.
Meakin, L.B., Price, J.S., Lanyon, L.E., 2014. The contribution of experimental in vivo models to understanding the mechanisms of adaptation to mechanical loading in bone. Front. Endocrinol. 5, 154.
Melville, K.M., Kelly, N.H., Khan, S.A., Schimenti, J.C., Ross, F.P., Main, R.P., van der Meulen, M.C., 2013. Female mice lacking estrogen receptor-alpha in osteoblasts have compromised bone mass and strength. J. Bone Mineral Res.
Morey-Holton, E.R., Globus, R.K., 2002. Hindlimb unloading rodent model: technical aspects. J. Appl. Physiol. 92, 1367–1377.
Morgan, E.F., Bayraktar, H.H., Yeh, O.C., Majumdar, S., Burghardt, A., Keaveny, T.M., 2004. Contribution of inter-site variations in architecture to trabecular bone apparent yield strains. J. Biomech. 37, 1413–1420.
Ozcivici, E., Garman, R., Judex, S., 2007. High-frequency oscillatory motions enhance the simulated mechanical properties of non-weight bearing trabecular bone. J. Biomech. 40, 3404–3411.
Patel, T.K., Brodt, M.D., Silva, M.J., 2014. Experimental and finite element analysis of strains induced by axial tibial compression in young-adult and old female C57Bl/6 mice. J. Biomech. 47 (2), 451–457.
Pereira, A.F., Javaheri, B., Pitsillides, A.A., Shefelbine, S.J., 2015. Predicting cortical bone adaptation to axial loading in the mouse tibia. J. R. Soc. Interface 12, 0590.
Razi, H., Birkhold, A.I., Weinkamer, R., Duda, G.N., Willie, B.M., Checa, S., 2015a. Aging leads to a dysregulation in mechanically driven bone formation and resorption. J. Bone Miner. Res. 30, 1864–1873.
Razi, H., Birkhold, A.I., Zaslansky, P., Weinkamer, R., Duda, G.N., Willie, B.M., Checa, S., 2015b. Skeletal maturity leads to a reduction in the strain magnitudes induced within the bone: a murine tibia study. Acta Biomaterialia 13, 301–310.
Riggs, B.L., Melton, L.J., Robb, R.A., Camp, J.J., Atkinson, E.J., McDaniel, L., Amin, S., Rouleau, P.A., Khosla, S., 2008. A population-based assessment of rates of bone loss at multiple skeletal sites: evidence for substantial trabecular bone loss in young adult women and men. J. Bone Miner. Res. 23, 205–214.
Robling, A.G., Burr, D.B., Turner, C.H., 2001. Skeletal loading in animals. J. Musculoskelet. Neuronal Interact. 1, 249–262.
Robling, A.G., Hinant, F.M., Burr, D.B., Turner, C.H., 2002. Improved bone structure and strength after long-term mechanical loading is greatest if loading is separated into short bouts. J. Bone Miner. Res. 17, 1545–1554.
Robling, A.G., Niziolek, P.J., Baldridge, L.A., Condon, K.W., Allen, M.R., Alam, I., Mantila, S.M., Gluhak-Heinrich, J., Bellido, T.M., Harris, S.E., Turner, C.H., 2008. Mechanical stimulation of bone in vivo reduces osteocyte expression of Sost/sclerostin. J. Biolog. Chem. 283, 5866–5875.
Rubin, C.T., Lanyon, L.E., 1984. Regulation of bone formation by applied dynamic loads. J. Bone Joint Surg. Am. 66-A, 397–402.
Silva, M.J., Brodt, M.D., Hucker, W.J., 2005. Finite element analysis of the mouse tibia: estimating endocortical strain during three-point bending in SAMP6 osteoporotic mice. The Anatom. Rec. Part A, Discov. Mol. Cell. Evol. Biol. 283, 380–390.
Silva, M.J., Brodt, M.D., Lynch, M.A., Stephens, A.L., Wood, D.J., Civitelli, R., 2012. Tibial loading increases osteogenic gene expression and cortical bone volume in mature and middle-aged mice. PloS One 7, e34980.
Sugiyama, T., Meakin, L.B., Browne, W.J., Galea, G.L., Price, J.S., Lanyon, L.E., 2012. Bones' adaptive response to mechanical loading is essentially linear between the low strains associated with disuse and the high strains associated with the lamellar/woven bone transition. J. Bone Miner. Res. 27, 1784–1793.
Sztefek, P., Vanleene, M., Olsson, R., Collinson, R., Pitsillides, A.A., Shefelbine, S., 2010. Using digital image correlation to determine bone surface strains during loading and after adaptation of the mouse tibia. J. Biomech. 43, 599–605.
Turner, C.H., 1998. Three rules for bone adaptation to mechanical stimuli. Bone 23, 399–407.
Weatherholt, A.M., Fuchs, R.K., Warden, S.J., 2013. Cortical and trabecular bone adaptation to incremental load magnitudes using the mouse tibial axial compression loading model. Bone 52, 372–379.
Willie, B.M., Birkhold, A.I., Razi, H., Thiele, T., Aido, M., Kruck, B., Schill, A., Checa, S., Main, R.P., Duda, G.N., 2013. Diminished response to in vivo mechanical loading in trabecular and not cortical bone in adulthood of female C57Bl/6 mice coincides with a reduction in deformation to load. Bone 55, 335–346.
Yang, H., Albiol, L., Chan, W.L., Wulsten, D., Seliger, A., Thelen, M., Thiele, T., Spevak, L., Boskey, A., Kornak, U., Checa, S., Willie, B.M., 2017a. Examining tissue composition, whole-bone morphology and mechanical behavior of Gorab(Prx1) mice tibiae: A mouse model of premature aging. J. Biomech. 65, 145–153.
Yang, H., Butz, K.D., Duffy, D., Niebur, G.L., Nauman, E.A., Main, R.P., 2014. Characterization of cancellous and cortical bone strain in the in vivo mouse tibial loading model using microCT-based finite element analysis. Bone 66, 131–139.
Yang, H., Embry, R.E., Main, R.P., 2017b. Effects of loading duration and short rest insertion on cancellous and cortical bone adaptation in the mouse Tibia. PloS one 12, e0169519.
Yang, H., Ma, X., Guo, T., 2010. Some factors that affect the comparison between isotropic and orthotropic inhomogeneous finite element material models of femur. Med. Eng. Phys. 32, 553–560.
Yang, H., Nawathe, S., Fields, A.J., Keaveny, T.M., 2012. Micromechanics of the human vertebral body for forward flexion. J. Biomech. 45, 2142–2148.